

Study of the population of neutron-rich heavy nuclei in the $A \sim 200$ mass region via multinucleon transfer reactions

E. Fioretto^{1,*}, L. Corradi¹, F. Galtarossa^{1,2}, S. Szilner³, D. Montanari⁴, T. Mijatović³, G. Pollarolo⁵, H.M. Jia⁶, D. Ackermann⁷, D. Bourgin⁴, G. Colucci⁸, S. Courtin⁴, G. Fruet⁴, A. Goasduff¹, J. Grebosz⁹, F. Haas⁴, D. Jelavić Malenica³, S.C. Jeong¹⁰, P.R. John⁸, M. Milin¹¹, G. Montagnoli⁸, N. Skukan³, F. Scarlassara⁸, N. Soić³, A.M. Stefanini¹, E. Strano⁸, V. Tokić³, C.A. Ur¹², J.J. Valiente-Dobón¹, and Y.X. Watanabe¹³

¹INFN, Laboratori Nazionali di Legnaro, I-35020 Legnaro (Padova), Italy

²Dipartimento di Fisica e Scienze della Terra, Università di Ferrara, I-44121 Ferrara, Italy

³Ruder Bošković Institute, HR-10002 Zagreb, Croatia

⁴Institut Pluridisciplinaire Hubert Curien, CNRS-IN2P3, Université de Strasbourg, F-67037 Strasbourg Cedex 2, France

⁵Dipartimento di Fisica Teorica, Università di Torino, and INFN Sezione di Torino, I-10125 Torino, Italy

⁶China Institute of Atomic Energy, P. O. Box 275(10), Beijing 102413, P. R. China

⁷Grand Accélérateur National d'Ions Lourds (GANIL), Boulevard Henry Becquerel, F-14076 Caen Cedex 5, France

⁸Dipartimento di Fisica dell'Università and INFN Sezione di Padova, I-35131 Padova, Italy

⁹The Henryk Niewodniczański Institute of Nuclear Physics, Polish Academy of Sciences, 31-342 Kraków, Poland

¹⁰Institute for Basic Science, Daejeon 305-811, Korea

¹¹Department of Physics, Faculty of Science, University of Zagreb, HR-10002 Zagreb, Croatia

¹²Horia Hulubei National Institute of Physics and Nuclear Engineering, RO-077125 Bucharest-Magurele, Romania

¹³Wako Nuclear Science Center, Institute of Particle and Nuclear Studies, High Energy Accelerator Research Organization (KEK), Wako, Saitama 351-0198, Japan

Abstract. Multineutron and multiproton transfer channels, populated in the inverse kinematics reaction $^{197}\text{Au}+^{130}\text{Te}$ at $E_{\text{lab}}=1.07$ GeV, were measured at Laboratori Nazionali di Legnaro using the presently heaviest ion beam delivered by the PIAVE-ALPI accelerator complex and detecting both projectile-like and target-like ions. To this end the large solid angle magnetic spectrometer PRISMA was coupled to a second arm for the detection of the heavy fragments in kinematic coincidence with the light ones selected and identified with the spectrometer. The data analysis is still in progress and will allow to compare the yields of both light and heavy partner with theoretical predictions performed with the GRAZING code to get quantitative information on transfer channels and the effect of evaporation and fission on the production rate of primary fragments. The mass integrated Z distribution, extracted from the experimental data, evidenced the population of proton pick-up channels that, in conjunction with the neutron stripping ones from the ^{130}Te , open the path for the production of neutron-rich heavy nuclei. In the following, we will present some preliminary results as well as details on the experimental configuration and perspectives for future investigations in the neutron-rich heavy region.

1 Introduction

On the basis of theoretical predictions, multinucleon transfer (MNT) processes in heavy-ion collisions around the Coulomb barrier have been proposed as a possible mechanism for the population of neutron-rich heavy nuclei [1], complementary to the fragmentation [2], opening new fields of research in nuclear physics such as the production and the study of the nuclear structure of unexplored exotic nuclei. In particular, there is presently a significant interest in the population of neutron-rich nuclei (in the mass region $A \sim 200$) located along the neutron closed shell $N = 126$ (the last waiting point in the r -path), having the largest impact on the astrophysical r -process [3, 4] and being crucial for understanding the shell evolution far

from the stability, and in the actinide region where nuclear structure information is important being the benchmark for theoretical models that provide predictions for the heaviest nuclei [5].

The feasibility of using MNT reactions around the Coulomb barrier for the production of neutron-rich heavy nuclei has been so far poorly investigated but recently benefited from the construction of new generation tracking spectrometers, based on the trajectory reconstruction and the use of the state-of-art large area particle detectors. The large acceptance of these spectrometers and the high resolving power of their detection systems gave a boost to this kind of studies. Different groups have recently started with or proposed measurements, focused on the determination of the heavy partner yield, in connection with the preparatory phases of facilities, such as KISS (KEK Iso-

*e-mail: fioretto@lnl.infn.it

tope Separator System) [6] at the Radiactive Isotope Beam Factory (RIBF) in RIKEN and GALS (Gas cell and Laser ion Separation) at the Joint Institute for Nuclear Research in Dubna [7], aiming to the study of β -decay spectroscopy of neutron-rich heavy nuclei in the $A \sim 200$ and $N \sim 126$ region populated via MNT. This information can be obtained either through γ -particle coincidence experiments [8], gating the light partner identified with high-resolution tracking spectrometers and measuring the yields of heavy partners via the associated γ -rays spectra Doppler corrected for the heavy partner, or via integral measurements of delayed β - γ coincidences [9]. As alternative technique, aiming to estimate the production rate of neutron-rich heavy nuclei, one can use a high-resolution kinematical coincidence. This technique is a powerful tool widely used for studying heavy-ion induced reactions from elastic and quasi-elastic to multinucleon transfer processes [10–13]. The method is mainly based on the simultaneous detection of the reaction fragments using two different set-ups placed at the kinematically correlated angles. The use of this technique in binary reactions allows to measure the yields of both partners getting information on the influence of secondary processes on the production rate of primary fragments.

In this framework, a benchmark experiment was recently carried out at LNL, aiming to measure the yields of light and heavy fragments populated in the inverse kinematics reaction $^{197}\text{Au}+^{130}\text{Te}$ at $E_{\text{lab}}=1.07$ GeV via MNT processes, by using the kinematical coincidence technique. The inverse kinematics method allowed to get a high detection efficiency and good mass and nuclear charge resolutions due to forward focusing of the reaction products and, for the present reaction, the higher kinetic energy of both binary partners at forward angles. This method has been already successfully applied in recent measurements performed with heavy-ion magnetic spectrometer PRISMA for the $^{96}\text{Zr}+^{40}\text{Ca}$ [14] and $^{116}\text{Sn}+^{60}\text{Ni}$ [15] systems aiming to the study of nucleon-nucleon correlation in the sub-barrier regime. The use of a ^{130}Te target (the most neutron-rich stable Te isotope) in conjunction with a ^{197}Au beam opens up both neutron stripping and proton pick-up channels, allowing the production of neutron-rich heavy nuclei in the $A \sim 200$ mass region, and proton stripping and neutron pick-up channels leading to the population of the benchmark nucleus ^{132}Sn . Because of the presence of fission and/or neutron evaporation that mainly affect the final yields of the heavy partner, it is extremely important to compare the experimental yields with theoretical predictions in order to estimate their effects in the regions of interest.

2 Experimental set-up

Correlated fragments produced in the interaction of a ^{197}Au beam with a thin ^{130}Te target were detected by using a kinematical coincidence set-up consisting of the large solid angle magnetic spectrometer PRISMA [16–18] (acting as main arm of the coincidence) coupled to an ancillary detection system acting as second arm, as displayed in figure 1.

PRISMA is the large acceptance magnetic spectrometer of LNL designed to be used for heavy-ion induced reactions at energies up to 10 AMeV. Its optical design consists of a magnetic quadrupole followed by a dipole with a bending angle of 60° and a curvature radius of 120 cm. The maximum magnetic rigidity amounts to 1.2 Tm. PRISMA is equipped with a position sensitive Micro-Channel Plate detector (MCP) [19] at the entrance of the spectrometer followed (at ~ 6 m of distance) by a large area focal plane detector [20]. The MCP, placed at 25 cm from the target, provides a timing signal for time-of-flight (TOF) measurements and X and Y position information. The focal plane detector is composed of a large area Multi-Wire Parallel Plate Avalanche Counter (MWPPAC), providing a timing signal and X and Y position information, followed by a transverse field segmented ionization chambers (IC), which allows the nuclear charge Z identification (based on ΔE - E technique) and the measurement of the energy loss ΔE_{IC} and total energy E_{IC} of the detected fragments. The timing signal of the PPAC is routinely used for time-of-flight (TOF) measurements with the MCP acting as start detector. The complete ion identification in PRISMA is performed through an event-by-event reconstruction of the trajectory inside the magnetic elements and the determination of the nuclear charge Z , the mass number A , the atomic charge state q , and the absolute velocity vector of each ion that reaches the focal plane detector.

The second arm consists of a Parallel Plate Avalanche Counter (PPAC) followed by an axial field ionization chamber, also known as Bragg chamber (BC) [21, 22]. This kind of ionization chamber allows to perform a Bragg curve spectroscopy, first proposed by Gruhn [23], providing simultaneously and with intrinsically high resolution many details about the nature of the fragments stopped in the active volume, such as the nuclear charge Z (due to the nearly linear dependence of the Bragg peak (BP) amplitude on Z), the range R (the length of the ion track) and the energy E of the fragments stopped in the active volume. The PPAC is composed of a central cathode and two anode planes orthogonally oriented on each side at a distance of 2 mm. The cathode is made of a double aluminized ($20 \mu\text{g}/\text{cm}^2 + 20 \mu\text{g}/\text{cm}^2$) Mylar foil with a thickness of $1.5 \mu\text{m}$. The anode planes consist of $10 \mu\text{m}$ diameter gold-plated tungsten wires 1 mm apart. The PPAC provides a fast timing signal and X and Y information with timing and position resolutions of the order of few hundreds ps and 1 mm, respectively. The BC has an active depth of 33 cm. The uniformity of the electric field in the active volume is obtained by means of 114 guard rings. The active volumes of PPAC and BC are separated by the entrance window of the ionization chamber, also acting as cathode, made of an aluminized ($20 \mu\text{g}/\text{cm}^2$) Mylar foil ($1.5 \mu\text{m}$). The BC was used to get simultaneously the nuclear charge Z_{BC} and the total energy E_{BC} of the fragments. The corresponding signals have been obtained by sending the output signal of the charge preamplifier to two amplifiers with shaping times of 0.25 and $4 \mu\text{s}$ for the amplitude of Bragg peak and the energy, respectively. The detection system was placed at ~ 90 cm from the target and had a geometrical solid angle quite similar to PRISMA (i.e. 80 msr).

3 Experiment details

The ^{197}Au beam was delivered by the PIAVE-ALPI superconducting accelerator complex of LNL with an intensity of 1.5 pnA and at an energy of $E_{lab}=1.07$ GeV. The target, isotopically enriched to 99.6% in ^{130}Te , with a thickness $200\ \mu\text{g}/\text{cm}^2$ (2 mm strip) was sandwiched between two $20\ \mu\text{g}/\text{cm}^2$ films of C in order to reduce the sputtering process on the target surfaces. Figure 1 shows the layout of the experimental set-up. PRISMA was placed around the grazing angle corresponding to $\theta_{lab}=37^\circ$ for the chosen bombarding energy. The coincident Au-like ions were detected with the second arm symmetrically placed with respect the beam axis at $\theta_{lab}=-37^\circ$. PRISMA and the second arm were connected to a sliding seal scattering chamber of 1 m diameter. Two Si detectors were mounted inside the scattering chamber at $\theta_{lab}=61^\circ$ and $\theta_{lab}=71^\circ$, respectively, in order to measure Rutherford scattered Te ions for the normalization of different runs and to monitor the beam quality during the experiment. A specific Ta beam stopper was designed to minimize the background in the entrance detector of PRISMA due to secondary electrons produced by the beam.

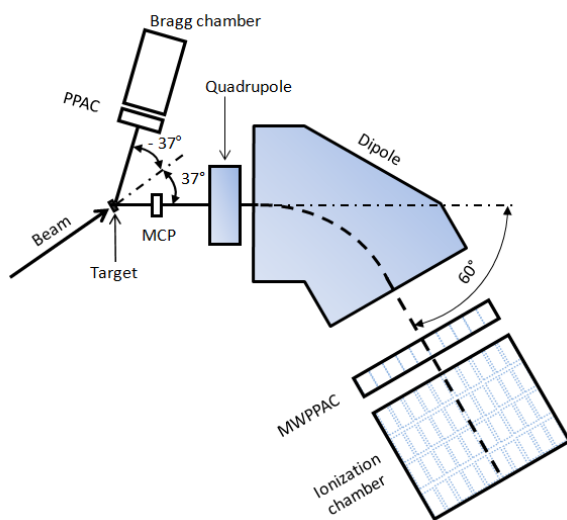


Figure 1. Sketch of the kinematic coincidence set-up used for the $^{197}\text{Au}+^{130}\text{Te}$ inverse kinematics reaction.

4 Light partner: PRISMA data

The magnetic spectrometer PRISMA and its focal plane detector were set in order to select and identify Te-like ions. The IC was operated with CH_4 as filling gas at a pressure of 93 hPa to stop target-like fragments in its active volume. In order to get a good Z resolving power, one has to properly take into account the direction followed by the different reaction products reaching the IC. In particular, the ion range R can be estimated from the signal of each IC section and the position information from MCP and MWPPAC. Figure 2 display the two-dimensional plot energy

E_{IC} vs range R measured with PRISMA detectors. The intense band which extends up to higher energies in the matrix corresponds to Te-like ions ($Z=52$) populated in binary reactions ranging from the quasi-elastic regime to more dissipative processes with increasing total kinetic energy losses (TKEL). Events located below this band in the same

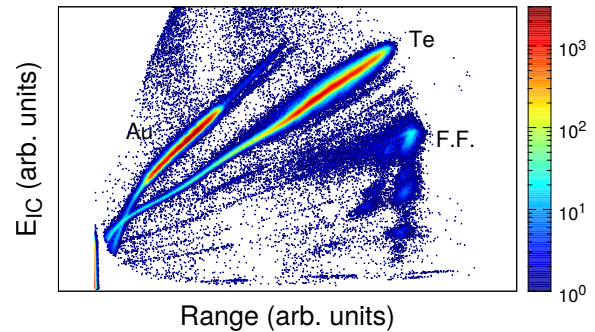


Figure 2. Energy E vs total range R of the ions detected at the focal plane of PRISMA for the $^{197}\text{Au}+^{130}\text{Te}$ reaction at $E_{lab}=1.07$ GeV.

figure have been associated to fission fragments (F.F.) produced in the reaction. They are not stopped in the active volume of the IC and, therefore show the characteristic punch-through effect in the matrix. Populated Au-like ions were almost stopped in the ΔE section and have an energy well below the threshold at which the Bragg peak occurs. The corresponding events are located in the intense band above the Te-like one. Due to the PRISMA settings, Au-like ions and fission fragments detected at the focal plane of the spectrometer correspond only to the ones having the correct p/q ratio (as the selected Te-like ions). As one can see in figure 2, the separation of the channels involving the transfer (stripping and pick-up) of few protons turned out to be very difficult due to the overwhelming of the elastic component. It is worthwhile to mention that in this experiment we chose a rather low bombarding energy (around the Coulomb barrier), in order to reduce the effect of secondary processes having in mind that the transfer yields, especially for proton transfer channels, may be modest. Figure 3 shows the mass integrated Z distribution corresponding to the nuclear species populated in the reaction. The estimated Z resolving power in this nuclear charge region was $\Delta Z/Z \sim 1/65$ that should be sufficient to distinguish different nuclear charges around $Z=52$, where the Te-like ions are located, confirming the good operation of the PRISMA IC. One observes the population of transfer channels involving both stripping and pick-up processes up to four protons. As expected from optimum Q -value considerations, the produced proton pick-up channels, are in the path of the population of neutron-rich heavy nuclei. One can also notice that the proton pick-up channels have yields larger than the corresponding proton stripping ones. The yields for the different channels will be extracted via a multigaussian fit of the experimental distribution.

For heavy ions around $A \sim 120-140$ the mass discrimination becomes difficult due to the decrease of the mass

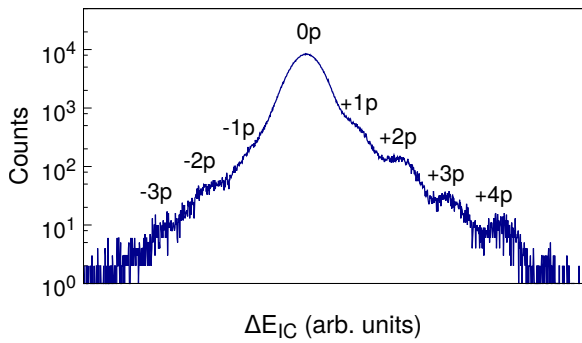


Figure 3. Mass integrated Z distribution of the fragments populated in the $^{197}\text{Au}+^{130}\text{Te}$ reaction at $E_{lab}=1.07$ GeV.

separation with increasing mass number. In addition, the mass resolving power of magnetic spectrometers may be affected by the presence of optical aberrations, especially for non-central trajectories, which have to be properly taken into account in the ion trajectory reconstruction, particularly for heavy masses. In order to reduce these effects and to improve the matching of the different sections of the focal plane detector, a dedicated off-line analysis was applied. This implied, in a first step, to tune the quadrupole length and the distance between target and quadrupole in order to take into account the effect of the fringing fields. Then, an iterative procedure was employed making use of the position information at the entrance and at focal plane of the spectrometer and performing a least-square fit of the A/q distributions with a n-order polynomial. From the resulting A/q distributions we extracted the mass spectrum summing over all atomic charge states. The outcome of this procedure is displayed in the mass A vs X position matrix of figure 4 showing the quality of the separation obtained for Te isotopes. This new procedure gave a mass resolving power of about $\Delta A/A \sim 1/240$. Even if both neutron pick-up and stripping were observed, the dominant flux was in the neutron stripping side, which was measured down to the $(-6n)$ channel. A similar situation

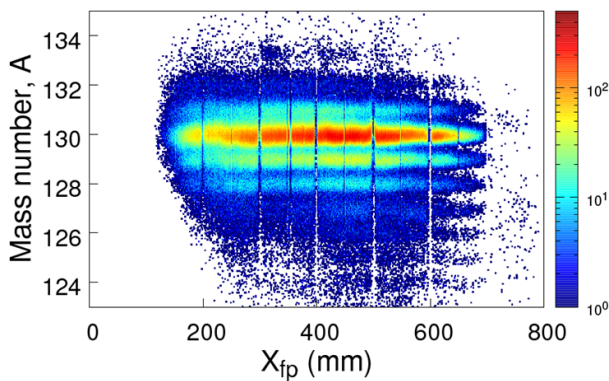


Figure 4. Mass number A vs X position scatter-plot obtained for Te isotopes.

was also observed in the recently measured $^{136}\text{Xe}+^{198}\text{Pt}$ [8] and $^{136}\text{Xe}+^{238}\text{U}$ [24] systems, making use of the most

neutron-rich stable ^{136}Xe isotope, and the $^{40}\text{Ar}+^{208}\text{Pb}$ reaction [25]. To learn more about the character of the final populated channels we have to compare them with theory. The on-going analysis will allow to extract the experimental yields and compare them with the theoretical predictions obtained with the GRAZING code [26, 27]. The model takes into account on the same footing surface degrees of freedom and particle transfer and the exchange of many nucleons proceeds via a multi-step mechanism of single nucleons (both, protons and neutrons, via stripping, and pick-up processes). The model has been so far successfully applied in the description of multinucleon transfer reactions [28–30] as well as of fusion reactions and barrier distributions [31].

In a dedicated run PRISMA was also set with correct magnetic fields and gas pressure in the IC in order to select and detect Au-like ions at the same angle $\theta_{lab}=37^\circ$. The main goal was to evaluate the channel identification also for very heavy ions [32]. Even if a good A/q resolution was obtained, the energy of Au-like ions was not sufficient to separate the different atomic charge states.

5 Heavy partner: kinematical coincidence data

In the kinematical coincidence measurement, the focal plane detector of PRISMA always acts as master trigger for the data acquisition system that has been implemented in order to include experimental information coming from the detectors of the second arm. These latter were optimized for the detection of the heavy partners. In particular, the BC was operated with CF_4 gas at a pressure of 53 hPa in order to stop Au-like ions into its active volume. It is worthwhile to stress that in the present experimental configuration light and heavy partners enter into the detectors of both PRISMA and the second arm. This can be observed in figure 5 that displays the E_{BC} (total energy measured with the Bragg chamber) vs ΔTOF (difference in TOFs between the PRISMA MCP and the PPAC of the second arm). One can see the excellent separation between Te-like and Au-like events identified imposing the coincidence condition in PRISMA. After several cross

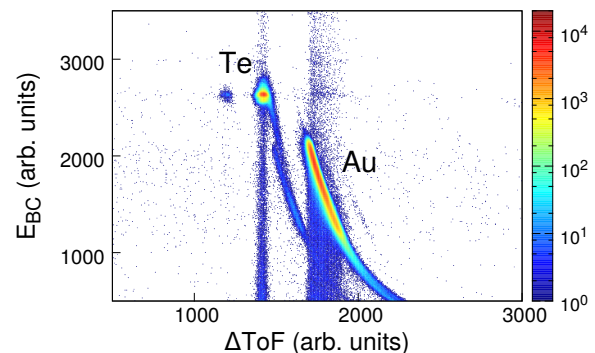


Figure 5. Scatter-plot energy E_{BC} , measured with the BC, vs ΔTOF between the PRISMA MCP and the PPAC in the second arm.

checks on the experimental spectra the correct operation of the kinematical coincidence was confirmed. We proceeded with the construction of the mass distribution of the heavy transfer products assuming a pure binary process and making use of the information on the correlated in-plane scattering angles as well as the difference in TOFs of the coincident fragments entering in the PRISMA MCP and the PPAC of the second arm. The obtained mass distribution is shown in figure 6, where the peaks are well centered at $A=197$ and $A=130$, corresponding to Au-like and Te-like ions, respectively. The mass resolution turned out to be $\Delta A/A \sim 1/43$. The construction of the mass-mass correlation matrix and its comparison with simulations, in order to estimate the effect of secondary processes, is in progress. The extracted cross sections for the heavy partner will be compared with theoretical calculations done with the GRAZING code.

6 Perspectives

The use of neutron-rich radioactive ion beams (RIB) that should be available, with reasonable intensity, in the forthcoming facility SPES [33] will provide important data to evaluate the possibility to access more exotic neutron-rich nuclei. As well known, transfer processes are mainly governed by form factors and optimum Q-value considerations. On the basis of theoretical predictions, transfer processes induced by neutron-rich RIBs on heavy targets will allow to populate neutron-rich heavy nuclei in the Pt-Os mass region with higher production cross sections. As an example, figure 7 displays the comparison of the estimated two-dimensional Z-A distributions for the heavy fragments populated in the reactions $^{136}\text{Xe}+^{198}\text{Pt}$ (upper panel) and $^{140}\text{Xe}+^{198}\text{Pt}$ (lower panel) at $E_{\text{lab}} = 850$ MeV. One can see the change in the population pattern from ^{136}Xe (the most neutron-rich Xe stable beam) to ^{140}Xe (neutron-rich RIB). The calculated production yield is not corrected by neutron evaporation, which of course limits the final yield of neutron-rich nuclei very far from stability.

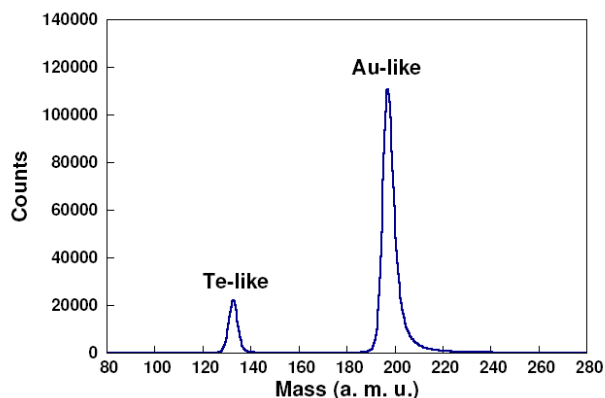


Figure 6. Mass distribution reconstructed with the kinematical coincidence. Light and heavy reaction products can be clearly distinguished.

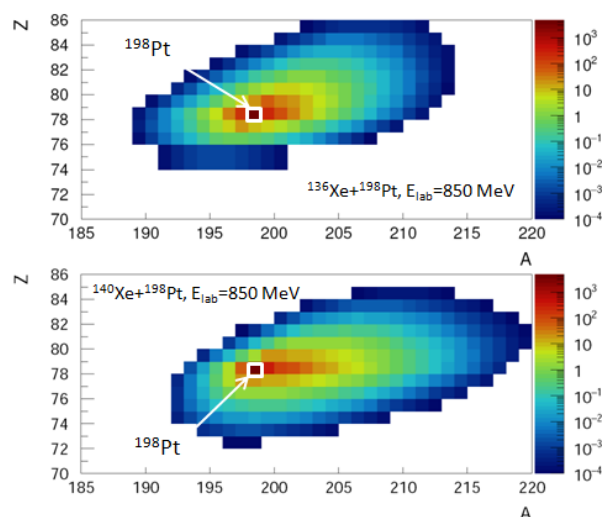


Figure 7. Total cross sections, calculated with the GRAZING code, for the heavy fragments populated in the $^{136}\text{Xe}+^{198}\text{Pt}$ (upper panel) and $^{140}\text{Xe}+^{198}\text{Pt}$ (lower panel) reactions at 850 MeV.

7 Summary

Recently the production of neutron-rich heavy nuclei around neutron magic number $N=126$ via MNT reactions has been focused theoretically and experimentally. In this framework, transfer channels populated in the inverse kinematics reaction $^{197}\text{Au}+^{130}\text{Te}$ were studied in a benchmark experiment by using the large solid angle magnetic spectrometer PRISMA coupled to a new gas detection system acting as second arm in a kinematical coincidence measurement. The population of neutron stripping and proton pick-up channels from ^{130}Te was evidenced. These processes open up the path leading to the production of neutron-rich heavy nuclei. The ongoing analysis will proceed with the extraction of the production cross sections for both light and heavy partner and their comparison with theoretical calculation performed with the GRAZING code. The mass spectrum of the heavy transfer products has been reconstructed by using the kinematical coincidence. This will allow to construct the mass-mass correlation matrix and compare it with simulations in order to estimate the effects of secondary processes, such as evaporation and fission. The extracted experimental yields for the heavy partner will also be compared with theoretical predictions obtained with the GRAZING code.

8 Acknowledgements

Grateful thanks are due to the staff of the Tandem/PIAVE-ALPI accelerator complex and to M. Loriggiola for preparing ^{130}Te strip targets of excellent quality. Funds for performing the research leading to the present results were received from the European Union Seventh Framework Programme FP7/2007- 2013 under Grant Agreement No. 262010 - ENSAR. This work was also partly supported by the Croatian Science Foundation under the project 7194.

References

- [1] C.H. Dasso, G. Pollarolo, A. Winther, Phys. Rev. Lett. **73**, 1907 (1994)
- [2] T. Kurtukian-Nieto *et al.*, Phys. Rev. C **89**, 024616 (2014)
- [3] K.-L. Kratz *et al.*, Astrophys. J. **403**, 216 (1994)
- [4] H. Grawe *et al.*, Rep. Prog. Phys. **70**, 1525 (2007)
- [5] V. Zagrebaev and W. Greiner, Phys. Rev. Lett. **101**, 122701 (2008)
- [6] Y. Hirayama *et al.*, Nucl. Instr. and Meth. B **352**, 4 (2015)
- [7] S. Zemlyanoy *et al.*, EPJ Web of Conferences **86**, 00067 (2015)
- [8] Y.X. Watanabe *et al.*, Phys. Rev. Lett. **115**, 172503 (2015)
- [9] K. Novikov *et al.*, J. Phys.: Conference Series **515**, 012016 (2014)
- [10] I. Tserruya *et al.*, Nucl. Instr. and Meth. **196**, 225 (1982)
- [11] G. Casini *et al.*, Nucl. Instr. and Meth. A **277**, 445 (1989)
- [12] H. Emling *et al.*, Nucl. Phys. A **211**, 600 (1973)
- [13] F.W.N. de Boer *et al.*, Z. Phys. A **325**, 457 (1986)
- [14] L. Corradi *et al.*, Phys. Rev. C **84**, 034603 (2011)
- [15] D. Montanari *et al.*, Phys. Rev. Lett. **113**, 052501 (2014)
- [16] A.M. Stefanini *et al.*, Nucl. Phys. A **701**, 217c (2002)
- [17] S. Szilner *et al.*, Phys. Rev. C **76**, 024604 (2007)
- [18] L. Corradi *et al.*, Nucl. Instr. and Meth. in Phys. Res. B **317**, 743 (2013)
- [19] G. Montagnoli *et al.*, Nucl. Instr. and Meth. in Phys. Res. A **547**, 455 (2005)
- [20] S. Beghini *et al.*, Nucl. Instr. and Meth. in Phys. Res. A **551**, 364 (2005)
- [21] E. Fioretto *et al.*, J. Phys: Conference Series **533**, 012006 (2014)
- [22] E. Fioretto *et al.*, EPJ Web Conf. **117**, 01004 (2016)
- [23] C.R. Gruhn *et al.*, Nucl. Instr. and Meth. **196**, 33 (1982)
- [24] A. Vogt *et al.*, Phys. Rev. C **92**, 024619 (2015)
- [25] T. Mijatović *et al.*, Phys. Rev. C **94**, 064616 (2016)
- [26] A. Winther, Nucl. Phys. A **572**, 191 (1994)
- [27] GRAZING code, <http://www.to.infn.it/~nanni/grazing>
- [28] L. Corradi, G. Pollarolo and S. Szilner, J. Phys. **G36**, 113101 (2009)
- [29] L. Corradi *et al.*, Phys. Rev. C **66**, 024606 (2002)
- [30] S. Szilner *et al.*, Phys. Rev. C **71**, 044610(2005)
- [31] G. Pollarolo and A. Winther, Phys. Rev. C **62**, 054611 (2000)
- [32] L. Corradi *et al.*, EPJ Web of Conferences **86**, 00007 (2015)
- [33] SPES: Selective Production of Exotic Species; <https://web.infn.it/spes/>